Strojniški vestnik - Journal of Mechanical Engineering 69(2023)7-8, 289-298
DOI:10.5545/sv-jme.2023.592
Original Scientific Paper
Received for review: 2023-03-30
Received revised form: 2023-05-03
Accepted for publication: 2023-05-31

The Dynamics of Tapered-roller Bearings – A Bottom-up Validation Study

Matej Razpotnik[1] - Thomas Bischof[2] - Miha Boltežar[1,*]
[1]University of Ljubljana, Faculty of Mechanical Engineering, Slovenia
[2]ZF Friedrichshafen AG, Germany

Rolling-element bearings are one of the most important elements when predicting the noise of rotating machinery. As a major connecting point between the rotating and non-rotating parts, their dynamic properties have to be accurately known. In this investigation we present a bottom-up approach to characterising the dynamics of the rolling-element bearing. A special test device was designed and built to assess the quality of the well-established analytical modelling approach of Lim and Singh. Two types of bearings were tested, i.e., the ball and tapered-roller types. The dynamic properties were observed by investigating the frequency-response functions. In addition, non-rotating as well as rotating test scenarios were checked. It was shown that the ball bearing model adequately predicts the system's response, whereas the tapered-roller bearing model requires modifications. These results were further confirmed with a quasi-static load-displacement numerical evaluation, where a full finite-element model serves as the reference.

Keywords: dynamic bearing model, tapered-roller bearing, bearing stiffness matrix, vibration transmission

Highlights

- *Test device for bottom-up investigation of bearing's dynamics is built.*
- *Ball and tapered-roller bearings are tested at different speeds and axial preloads.*
- *The system is evaluated numerically and experimentally.*
- *Ball bearing model is validated whereas tapered-roller one needs improvements.*

0 INTRODUCTION

Every rotating machinery contains bearings. They represent the connecting points between the rotating and non-rotating parts and so are very important elements in the chain of vibration transmission. The dynamic properties of rolling-element bearings have been studied for many decades; however, due to their complex contact-related phenomena the topic remains important in ongoing research.

A first general theory for elastically constrained ball and roller bearings was developed by Jones [**1**]. Later this theory was further extended by Harris [**2**]. The theory was very general and focused more on static and fatigue-life calculations than on the vibration transmission through the bearings. Simplified bearing models were introduced by other researchers, with the bearings being modelled as an ideal boundary condition for the shaft, as presented by Rao [**3**]. Meanwhile, the idea of interpreting the bearings with a simple one- or two-degrees-of-freedom (DOFs) model with linear springs was introduced by While [**4**] and Garigiulo [**5**]. Later, more accurate dynamic bearing models were derived. A major improvement in predicting the vibration transmission through rolling-element bearings was made by Lim and Singh [**6**] and [**7**] and in parallel by de Mul [**8**]. They derived a model that provides a comprehensive bearing-stiffness matrix. The model is capable of describing the nonlinear relation between the load and the deflection, taking into account all six DOFs and their interplay. These authors also presented system studies [**9**] and [**10**] for model-validation purposes. A good agreement between the measurements and the analytical model was shown for the ball and the cylindrical roller bearings as the two most distinct examples of different contact types. The six-DOFs model is the basis for the widely used industrial standard ISO/TS 16281 [**11**] as well as for many subsequent studies. Recently, a thorough review of mechanical model development of rolling-element bearing was presented by Cao et al. [**12**]. The authors classify modelling approaches into five different techniques and comprehensively discuss the current progress of development as well as identify future trends for research. Despite great computational power available these days, modelling of the bearings primary remains on the analytical level. Contact related phenomena and non-linearities lead to huge and often unstable finite-element method (FEM) models. However, connecting analytical models with numerical ones is crucial in predicting the proper behaviour of a modern system. Guo and Parker [**13**] presented a stiffness-matrix calculation

*Corr. Author's Address: University of Ljubljana, Faculty of Mechanical Engineering, Aškerčeva 6, 1000 Ljubljana, Slovenia, miha.boltezar@fs.uni-lj.si

using a finite-element/contact-mechanics model. On the other hand analytical approaches demand advanced methods to solve the system of nonlinear equations. Fang et al. [14] recently presented a comprehensive study of the speed-varying stiffness of ball bearings under different load conditions. They proposed a novel mathematical method for solving an implicit set of nonlinear equations based on a new assumption of the initial conditions. To mitigate the numerical difficulties of time integration procedure, induced by rolling-elements coming and leaving the contact, Razpotnik et al. [15] extended the model from Lim and Singh [6]. They implemented modular smoothing of the load-displacement characteristics in the region of contact-state transition. To improve the calculation accuracy of non-hertzian contact pressure the high-precision half space theory was adopted by Kabus et al. [16] and [17].

Tapered-roller bearings (TRBs) are widely used in rotor dynamics. They are usually treated as a special case of a cylindrical roller bearing with a non-zero contact angle. The difference, in fact, is much more significant because TRBs have two different contact angles (the inner ring-roller and outer ring-roller contacts) and also because of their additional roller-flange contact. Cretu et al. [18] and [19] analysed the dynamics of TRBs under fully flooded conditions. The assumption of an elastohdydrodynamic (EHD) lubrication regime is common to the majority of TRB studies. In this way the friction forces can be either calculated or, even more commonly, neglected. Tong and Hong [20] analytically studied the characteristics of TRBs subjected to combined radial and moment loads. The same authors [21] investigated the influence of the roller profile and the speed on the stiffness of a TRB. Zhao et al. [22] studied the effect of gyroscopic moment on the damage of a tapered-roller bearing, which are found to occur under high-speed and high-load conditions, such as high-speed trains. Roda-Casanova and Sanchez-Marin [23] presented an illustrative study of the contribution of the deflection of the TRB to the misalignment of the pinion in a pinion-rack transmission. They stressed the importance of having accurate knowledge of the elasticity of the bearings. Houpert [24] studied the torque generated by the friction forces in a TRB, where he emphasised an important fact, i.e., TRBs are subjected to a high roller-flange torque. The roller-flange contact, which largely affects the power loss, was investigated also by Ai et al. [25]. In addition, Tong et al. [26] made numerical evaluation of the effect of misalignment on the generated friction forces and consequently evaluated the power loss of a TRB. It was shown that already a small misalignment can have a significant influence on the generated torque.

Experimental investigations of a TRB's dynamics are rare in the literature. Zhou and Hoeprich [27] measured the torque generated at different contacts in a TRB; however, they focused on the losses and not on the dynamics. Gradu [28] also analysed the TRB losses and compared them with equivalent ball bearing. Wrzochal et al. [29] presented a new device for measuring the friction torque in rolling-element bearings of different types, where the main goal was to establish a reliable device for quality control measurement. Discrepancy between theoretical and measured friction torque was presented and discussed. A comparative study, as presented by Zhang et al. [30] for angular-contact ball bearings, would also be beneficial for TRBs. Further, since TRBs are often used in applications that do not require high speed, the influence of friction on the dynamic properties would be generally welcomed.

In this paper a numerical and experimental characterisation of a TRB's dynamics is presented. First, a general bearing modelling technique is introduced, where the analytical model of Lim and Singh [6, 7] is embedded into a FEM model. Afterwards, a special test device is presented. There follows a description of a workflow for a bottom-up validation study. A TRB is mainly investigated, whereas ball bearing is also tested. The results in the form of frequency-response functions (FRFs) are compared for the measurements and the simulations. The non-rotating as well as low-speed-rotating scenarios are presented. Finally, a quasi-static load-displacement numerical analysis was performed to additionally verify the results.

1 BEARING MODELLING TECHNIQUE

Rolling-element bearings can be modelled as a part of a wider system in several different ways. Most often the system is studied by utilising a FEM model. The bearings are, due to their complex contact-related phenomena, represented by a special element that embeds the analytically calculated bearing-stiffness matrix $\mathbf{K}_b$. This technique introduces the so-called spider elements (commercially known as RBE3 element), as shown in Fig. 1. A spider element connects a raceway of a ring to one, central node. The motion of that central node depends on the weighted average of the motions at a set of connected grid points [31]. Two spider elements are needed,

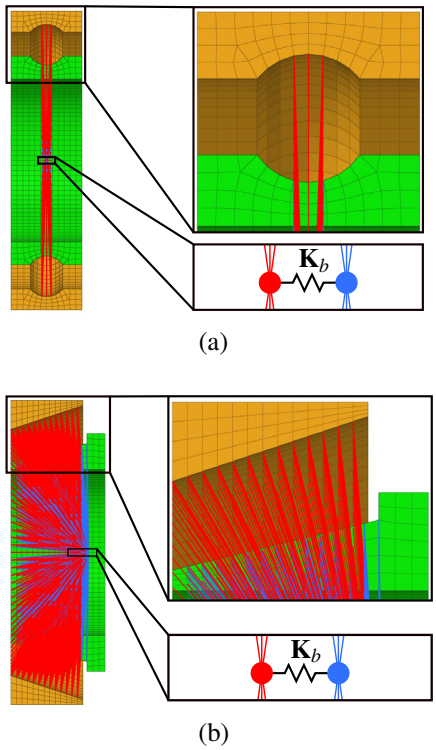

Fig. 1. *A cross-section view of a bearing in a FEM model with zoomed-in areas; a) ball bearing, and b) TRB*

each for one bearing ring. Central nodes, connected by $\mathbf{K}_b$, are located at exactly the same position. Fig. 1 separates them just for illustrative purposes. Bearing rings can be coarsely meshed since the mesh is only used to represent the shape of the ring and to serve as a connecting body for the spider element. Rolling elements are not modelled, since all contact-related phenomena are covered by the stiffness matrix. The source of the accuracy of the presented technique is not in the spider element itself, but in the bearing-stiffness matrix. In this study we implement the bearing-stiffness matrix from Lim and Singh [**6**] and [**7**]; however, any relevant bearing theory yielding the stiffness matrix can be implemented.

There are two types of FEM analyses used in the presented study, i.e., frequency-response modal analysis and quasi-static load-displacement analysis. Both assume that rolling elements are not rotating. However, the former is used to obtain dynamic response of the system when excited and subjected under different axial loads, and the latter is used to obtain load-displacement characteristics of a bearing.

2 TEST DEVICE

A simple test device was designed and built for validation purposes. It consists of the housing, a long shaft and a special nut, as shown in Fig. 2. It is important to note the shape of the nut, which is only in contact at both ends. This design ensures that the load dependency of the thread contact is negligible. A bottom-up validation approach was utilised. Therefore, solid rings are inserted at first in order to prove the linearity of the system. Afterwards, two types of rolling-element bearings were tested, i.e., ball bearing and TRB, with the properties given in Table 1. In order to eliminate the influence of the surroundings, the device was tested with free-free boundary conditions (BCs). These conditions were achieved by hanging the test device via housing by thin ropes. The FRFs were measured between different parts of the system. An excitation was applied with a modal hammer, whereas the acceleration was measured by the accelerometer. The transfer path from the shaft to the housing is of special interest, since the bearing's dynamics are the most clearly seen there. The test device makes it possible to apply different axial preloads to the bearings and consequently to the entire system by turning the nut with respect to the shaft. The applied axial force is measured with the strain gauges located at the housing ribs. Additionally, the system can be investigated while the shaft is either stationary or rotating (up to 6000 rpm). For this purpose a special motor can be mounted to the system. In doing so, the free-free BCs are maintained, as shown in Fig. 3.

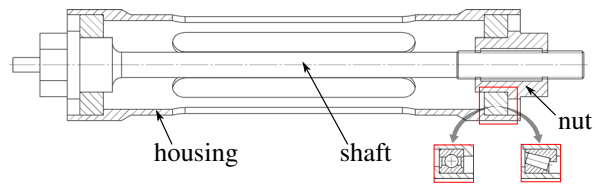

Fig. 2. *A simplified technical drawing of the test device, where all three possible configurations are shown*

Table 1. *Bearings used in the test device.*

type	designation	d [mm]	D [mm]	B [mm]
ball	6006	30	55	13
tapered-roller	32006-X	30	55	17

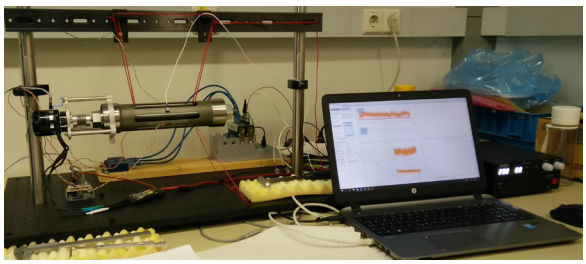

Fig. 3. *Experimental setup with attached motor*

3 WORKFLOW

The main goal was to evaluate the quality of the analytically calculated dynamic bearing model. The assessment was made for a non-rotating scenario by comparing the dynamic properties of the system in the form of FRFs. We focused on a representative FRF, namely Accelerance, where the excitation was performed on the shaft and acceleration was obtained at the housing, as shown in Fig. 4. All of the possible setups (solid rings, ball bearings, TRBs) undergo the same testing procedure. Four different axial preloads were inserted into the system. Thus, four different FRFs were obtained. Fig. 5 shows

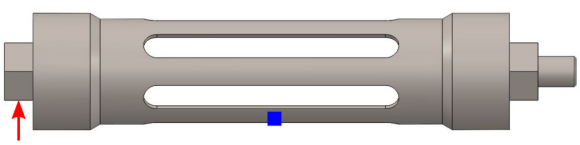

Fig. 4. *Excitation point and accelerometer position*

the corresponding workflow. The same workflow is followed for measurements and simulations. Finally, the FRFs are compared.

The rotating version of the test device was investigated only experimentally. A run-up investigation was utilised. By that we can see the potential change of the system's dynamics due to rotor-dynamic effects appearing in the rolling bearings, e.g., centrifugal forces and gyroscopic effects. Some researchers have pointed out these effects during high-speed applications [**1**], [**14**], [**21**], [**22**], and [**32**], where the effects start to become noticeable in the region between 5000 rpm and 10000 rpm, depending on the bearing type and load case. However, it is important to note that our testing did not exceed 6000 rpm. When the system rotates, there is no additional external excitation. The system is mainly excited by the white noise coming from the bearings. The resulting acceleration is measured and shown in a Campbell diagram.

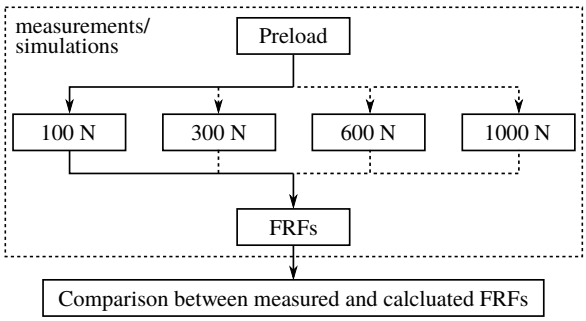

Fig. 5. *Workflow of the validation procedure for the non-rotating test device*

4 RESULTS

4.1 Solid Rings

With solid rings inserted it is possible to verify whether the system without bearings is linear or not. The linearity implies the load-independent dynamic properties of the system. Ideally, the presented system should be load-independent; however, due to contact issues, especially the thread contact, the load independence has to be experimentally proven. Fig. 6 shows the results. The measured FRFs, given in the form of Accelerance (A), are shown with a gray and black colour. The red curve corresponds to simulation. The preload was considered in simulations as well, but its effect is completely unnoticeable, thus only one line sufficiently represents the simulation results. It is clear that all the measured curves correlate well with each other regarding the eigenfrequency position. Damping, however, decreases with an increased preload. Also, the calculated FRF predicts the measured behaviour correctly. However, the peak around 1.45 kHz is more damped in the measured results.

Proving the linearity of the system with solid rings is an important step. All the non-linearities in the succeeding investigations (when real bearings are inserted) can now be associated with the bearing's behaviour.

4.2 Ball Bearings

The ball bearings, as given in Table 1, are inserted into the system. Fig. 7 shows the amplitude comparison between the measured and calculated results. It is clear that some peaks move their position with the increased preload, while the others do not. Those involving the modes of the shaft are affected, while the others are not. Fig. 8 shows the modes of the marked regions from Fig. 7. The stiffness of the bearing plays a crucial role there. All of them are pure modes of the shaft, only the mode at 2490 Hz is a combination

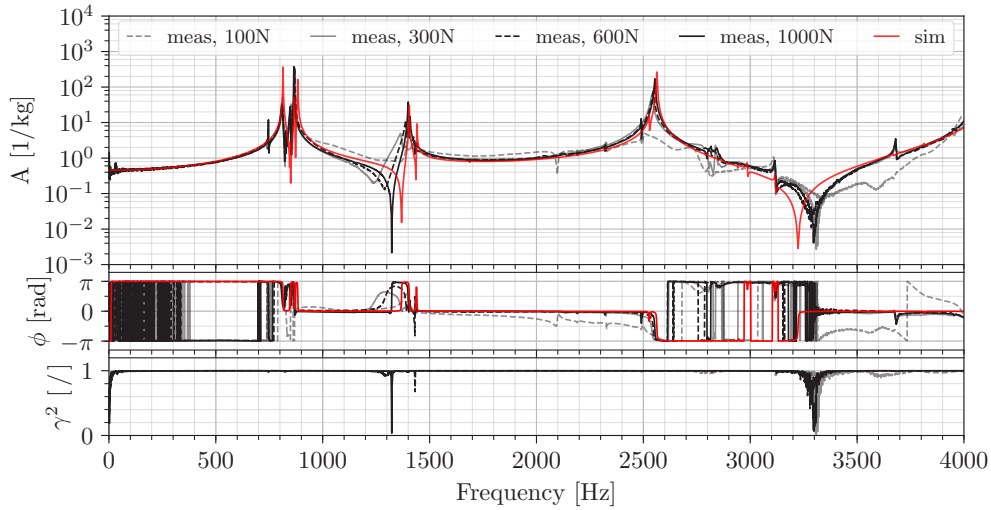

Fig. 6. *Load-dependency of the FRF (from top to bottom: magnitude, phase, coherence) for the test device with the inserted solid rings*

of shaft and the local movement of the housing ribs. Additionally, it is clear that the higher the preload, the higher is the bearing stiffness. This also causes the eigenfrequencies to increase. Comparing the spectra it can be seen that the frequency span of each affected eigenfrequency is around 100 Hz for the measured as well as the calculated FRFs. Some peak positions, however, differ slightly, but the general behaviour is well predicted. It is important to note that no FEM model updating was performed. Doing so would obviously align the calculated results completely with the measured ones.

So far, we have presented the non-rotating version of the test device. Since the bearings are meant to rotate it is crucial to determine whether the analytical bearing-stiffness matrix is an adequate representation of the bearing's dynamics also under operating conditions. A run-up test was performed. An extension to the motor was additionally mounted to the test device while maintaining its free-free BCs (see Fig. 3). The run-up test sequentially increases the motor speed from 500 rpm to 6000 rpm with a step of 100 rpm. At each step the acceleration on the housing (the same position as for the FRF investigation) was measured. The resulting Campbell diagram is shown in Fig. 9 for the preloads of 300 N and 1000 N. The preload of 100 N was found to be too loose for the run-up investigation. Already a slight torque induced by the motor caused a disturbance that changed the axial preload. At 300 N this effect is not noticeable any more. It is clear that the eigenfrequencies governed by the bearing stiffness do change with a higher preload in a similar manner to the non-rotating version. They are marked with red arrows. On the other hand, their position does not change while increasing the RPM in the investigated RPM region. Another important conclusion is that the locations of the eigenfrequencies remain at practically the same positions as in the non-rotating investigation.

The distinct change of eigenfrequencies dominated by the bearing stiffness is evident. Comparing the results for the non-rotating and rotating versions we notice that one dominating peak is missing in the rotating version, i.e., the one at 2490 Hz. The eigenmode of this peak is a combination of housing and shaft movements and is apparently changed due to the extension mounted to the housing.

The comparison between the measurements and the simulations shows good agreement for the non-rotating as well as for the rotating setup. As such it can be concluded that the analytical bearing-stiffness matrix seems to be an adequate representation of the actual bearing's dynamics for the ball type in the observed speed range.

4.3 Tapered-roller Bearings

The TRBs, as given in Table 1, are inserted into the system. Fig. 10 shows the amplitude comparison between the measured and calculated results. Both spectra have marked regions where the eigenfrequencies shift with respect to the inserted preload. Comparing the spectra it is clear that the positions of the regions differ tremendously. Investigating the eigenmodes gives us an insight into the problem. Fig. 11 shows all the calculated eigenmodes of the test device within the marked

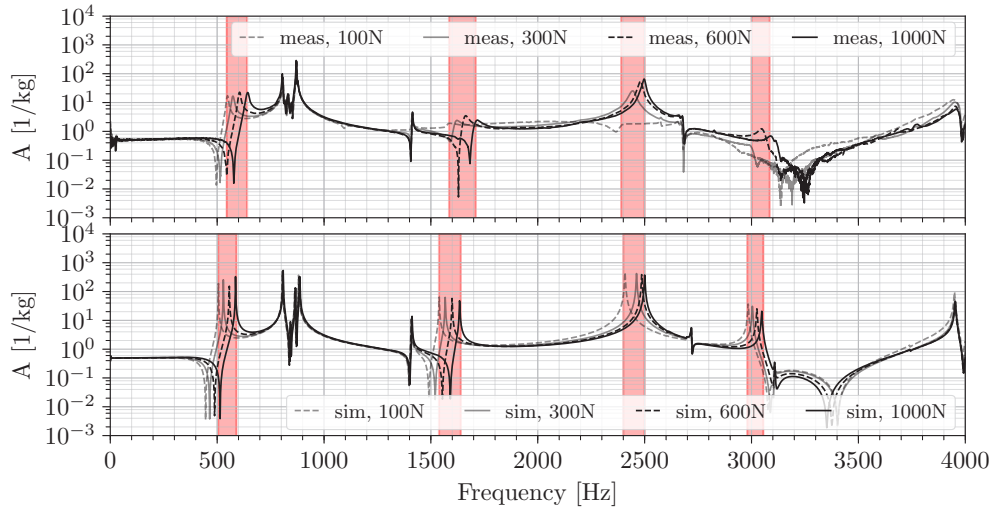

Fig. 7. *Comparison between the measured (upper part) and calculated (lower part) load-dependency of the chosen FRF for the test device with inserted ball bearings*

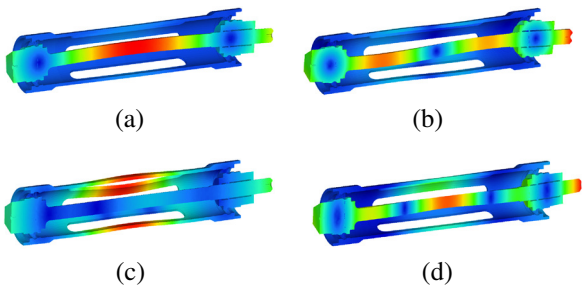

Fig. 8. *Selected calculated eigenmodes of the test device with ball bearings; a) Eigenmode at 590 Hz, b) Eigenmode at 1650 Hz, c) Eigenmode at 2490 Hz, and d) Eigenmode at 3085 Hz*

frequency band from Fig. 10. All the presented modes are governed by the bearing stiffness and do actually correspond to the first, second and third modes of the shaft. To show the measured modes we need to do a complete experimental modal analysis (EMA). For this purpose we used an approach with a high-speed camera. The measured eigenmodes are shown in Fig. 12. The first eigenmode obviously represents the first mode of the shaft, whereas the second mode represents the combination of the dominant local housing movement and the second mode of the shaft. The arrows in Fig. 12 indicate the direction of motion, where a different colour stands for a different phase. From the presented results it can be concluded that the analytically calculated bearing-stiffness matrix for the TRBs exhibits behaviour that is much too weak. As such the current modelling approach is not an adequate representation of the TRB's dynamics.

Since the non-rotating scenario has a huge gap between the measurements and the calculations we did not continue to the rotating scenario. Instead we tried to shed some light on possible causes for the observed differences with the help of a detailed FEM bearing model, as discussed in detail in the next section.

5 NUMERICAL INSIGHT

The analytical bearing-stiffness model seems to be a good representation of reality for the ball bearing, but considerably worse for the TRB. To find the origin of the problem we built a complete, detailed, full FEM bearing model for both bearing types (see Table 1) as depicted in Fig. 13. The goal is to compare the load-displacement characteristics, where the load is exerted incrementally in the axial direction. A quasi-static load-displacement analysis was performed on the full FEM bearing model. Further, the slope of the load-displcement curve is extracted, representing the total axial stiffness in the loaded direction, which is also compared. Due to its completeness, the FEM model represents the reference. Besides the full FEM model and the analytical model from Lim and Singh [**6**] and [**7**], the results from the widely used standard ISO/TS 16281 [**11**] are also included.

The results in the form of load-displacement characteristics and the corresponding stiffness for the ball bearing are shown in Fig. 14. All three approaches result in similar characteristics. There is a minor gap between both analytical approaches, whereas the FEM yields a slightly higher stiffness at a high preload.

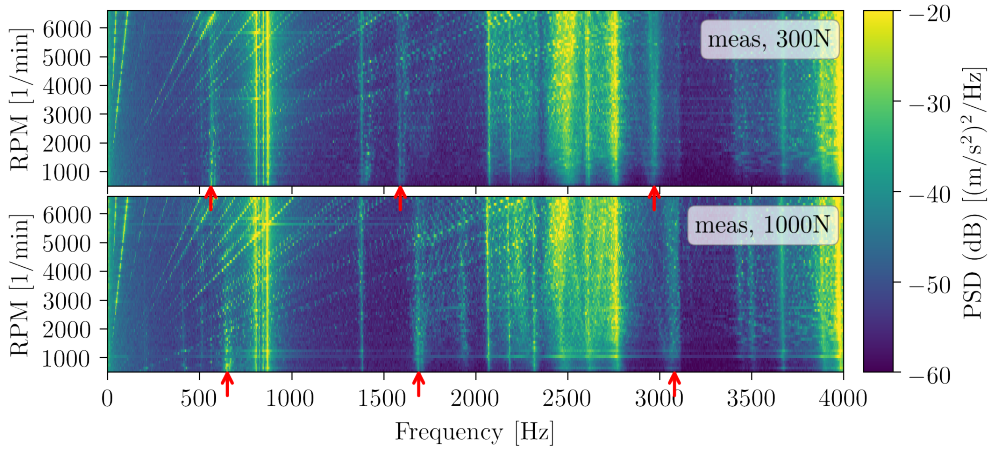

Fig. 9. *Campbell diagrams for the test device with inserted ball bearings loaded under 300 N and 1000 N*

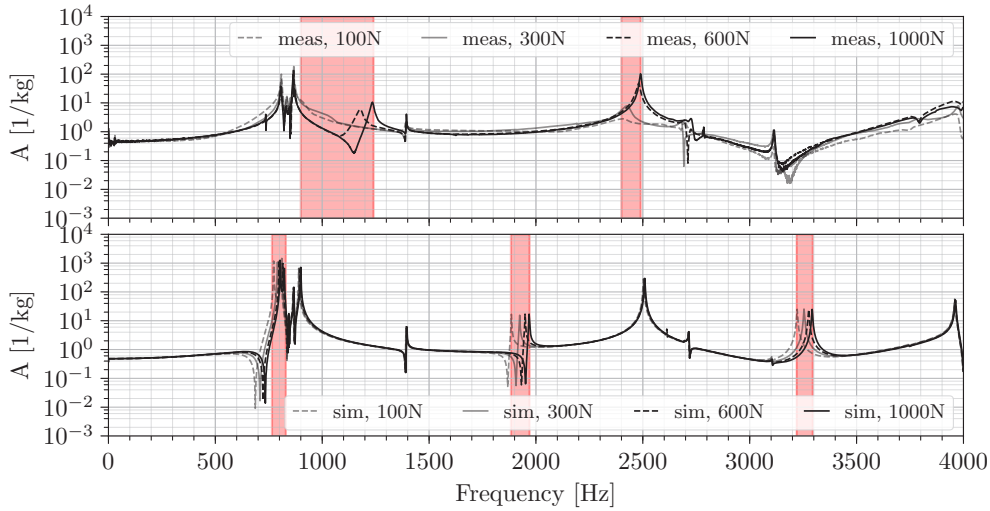

Fig. 10. *Comparison between the measured (upper part) and calculated (lower part) load dependency of the chosen FRF for the test device with inserted TRBs*

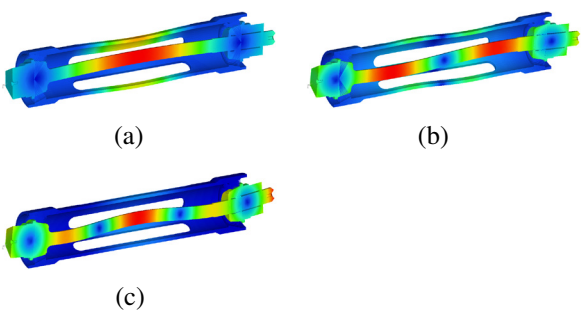

Fig. 11. *Selected calculated eigenmodes of the test device with TRB; a) Eigenmode at 820 Hz, b) Eigenmode at 1960 Hz, c) Eigenmode at 3300 Hz*

However, it can be concluded that all the models are sufficiently well correlated.

In the same manner we incrementally load the TRB in the axial direction. The results are shown in Fig. 15. The curves quantitatively differ significantly; however, they reflect the same tendency. Concerning the load-displacement characteristics, it is interesting that already both analytical approaches differ to a great extent. The same two approaches exhibit a similar level in the stiffness characteristic. The FEM model, on the other hand, yields a factor of two higher stiffness.

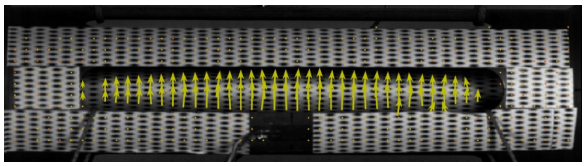

(a)

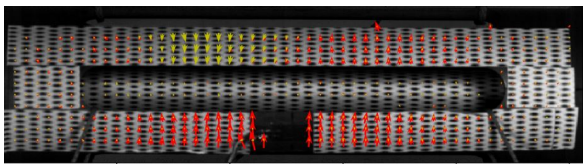

(b)

Fig. 12. *Measured eigenmodes of the test device with inserted TRB (using high-speed camera); a) Eigenmode at 1250 Hz, b) Eigenmode at 2490 Hz*

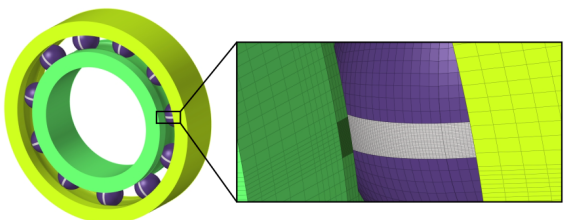

(a)

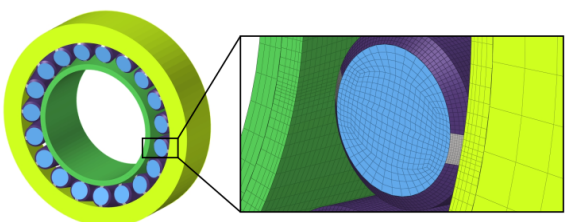

(b)

Fig. 13. *Full FEM model of a bearing; a) ball bearing, b) TRB*

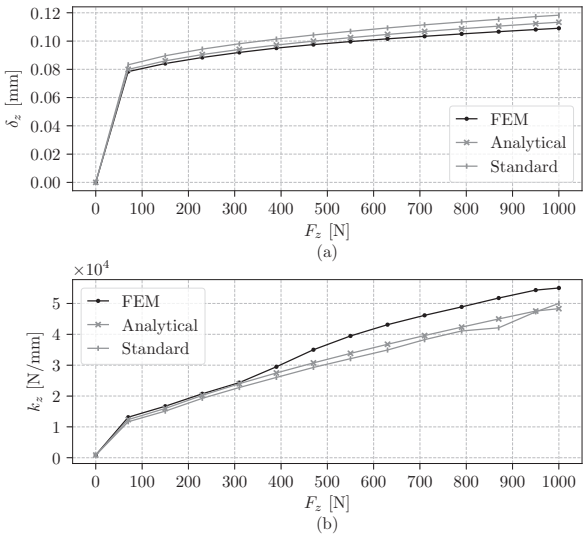

Fig. 14. *Ball bearing being incrementally loaded in the axial direction; a) load-displacement characteristic, b) corresponding total stiffness*

6 DISCUSSION

Modelling the dynamics of ball bearings with the presented approach seems appropriate. The discrepancy between the measurements and the simulations is negligible. On the other hand, the TRBs have a significant mismatch between the measured and calculated results. This is true for the dynamic testing (comparing FRFs) as well as for a simple quasi-static load-displacement investigation. The reason for such a disagreement is the inadequate bearing-stiffness model. The shortcomings can be outlined as:

1. The TRB has different contact angles in between the inner ring-roller and the outer ring-roller. The theory assumes that all the contacts are happening at the nominal contact angle, which is defined for the axis going through the centre of a roller. Consequently, no axial force is generated that pushes the rollers out of the initial contact and no flange is needed to prevent the rollers from escaping the contact. The roller-flange contact is thus neglected. This contact carries only minimal load; however, it should not be neglected, especially if the TRB is loaded in the axial direction only. It is important to note that the literature provides some theories that take into account different contact angles and flange contacts [**8**] and [**21**]. However, those theories provide a negligibly different stiffness matrix compared to the theory, which does not include the mentioned contacts. Having looked at the results, the stiffness should be of factorial difference.

2. Friction effects are neglected in all models, i.e., analytical, standard and FEM model. When the bearing operates in the hydrodynamic regime, the friction is expected to be very small and as such it is justified to neglect it in the stiffness calculation. However, when the bearing operates in the boundary or mixed-lubrication regime, the friction coefficients are expected to have a significant influence on the bearing's stiffness. Further, the dynamic load from the eigenmodes is expected to be small enough to not cause the transition from the stick to the slip state in the contact along the roller's line of action. That

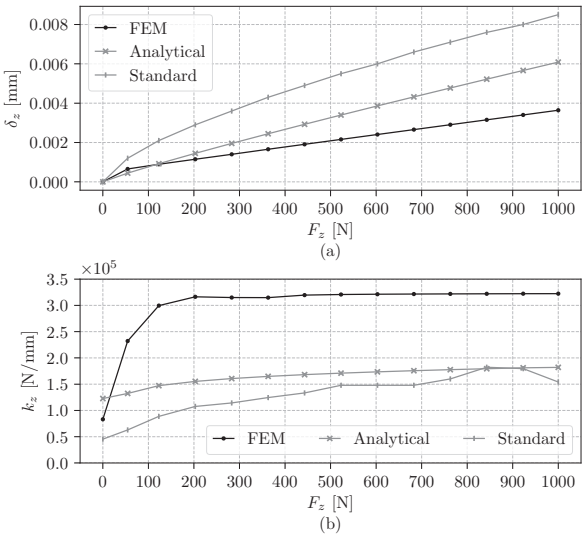

Fig. 15. *TRB being incrementally loaded in the axial direction; a) load-displacement characteristic, b) corresponding total stiffness*

being said, the stiffness of the TRB would have been significantly increased when the friction phenomena were also taken into account.

7 CONCLUSION

A bottom-up approach to characterise a bearing's dynamics is presented. A special test device was designed and built to assess the quality of the well-established modelling approach. The dynamic properties of the system were measured in the form of FRFs, where load-dependent nonlinearities, resulting from the bearings were observed. It was shown that the ball bearing model yields appropriate results, whereas the TRB model requires modifications. These outcomes were confirmed with a quasi-static, load-displacement numerical insight, where a full FEM model serves as a reference.

In future work it will be of great interest to see how a TRB reacts when loaded in other than the pure axial direction. In addition, the influence of a different lubrication regime would shed some light on questions relating to the friction. The presented study represents a good starting point for a possible new TRB model derivation.

8 ACKNOWLEDGEMENT

The authors would like to thank the ZF Friedrichshafen AG for supporting this research.

9 REFERENCES

[1] Jones, A.B. (1960). A general theory for elastically constrained ball and radial roller bearings under arbitrary load and speed conditions. *Journal of Basic Engineering*, vol. 82, no. 2, p. 309-320, **DOI:10.1115/1.3662587**.

[2] Harris, T.A. (1984). *Rolling Bearing Analysis*, John Wiley, New York.

[3] Rao, J.S. (1983). *Rotor Dynamics*, John Wiley, New York.

[4] While, M.F. (1979). Rolling element bearing vibration transfer characteristics: Effect of stiffness. *Journal of Applied Mechanics*, vol. 46, no. 3, p. 677-684, **DOI:10.1115/1.3424626**.

[5] Gargiulo, E.P. (1980). A simple way to estimate bearing stiffness. *Machine Design*, vol. 52, p. 107.

[6] Lim, T.C., Singh, R. (1990). Vibration transmission through rolling element bearings, part 1: Bearing stiffness formulation. *Journal of Sound and Vibration*, vol. 139, no. 2, p. 179-199, **DOI:10.1016/0022-460X(90)90882-Z**.

[7] Lim, T. C., Singh, R. (1994). Vibration transmission through rolling element bearings, part 5: Effect of distributed contact load on roller bearing stiffness matrix. *Journal of Sound and Vibration*, vol. 169, no. 4, p. 547-553, **DOI:10.1006/jsvi.1994.1033**.

[8] Mul, J. M., Vree, J.M., Maas, D.A. (1989) Equilibrium and Associated Load Distribution in Ball and Roller Bearings Loaded in Five Degrees of Freedom While Neglecting Friction-Part I: General Theory and Application to Ball Bearings. *Journal of Tribology*, vol. 111, no. 1, p. 142-148, **DOI:10.1115/1.3261864.**

[9] Lim, T.C., Singh, R. (1990). Vibration transmission through rolling element bearings, part 2: System studies. *Journal of Sound and Vibration*, vol. 139, no. 2, p. 201-225, **DOI:10.1016/0022-460X(90)90883-2**.

[10] Mul, J.M., Vree, J.M., Maas, D.A. (1989). Equilibrium and associated load distribution in ball and roller bearings loaded in five degrees of freedom while neglecting friction-Part II: Application to roller bearings and experimental verification. *Journal of Tribology*, vol. 111, no. 1, p. 149-155, **DOI:10.1115/1.3261865**.

[11] ISO/TS 16281:2008. *Rolling Bearings - Methods for Calculating the Modified Reference Rating Life for Universally Loaded Bearings*. International Organization for Standardization, Geneva.

[12] Cao, H., Niu, L., Xi, S., Chen, X. (2018). Mechanical model development of rolling bearing-rotor systems: A review. *Mechanical Systems and Signal Processing*, vol. 102, p. 37-58, **DOI:10.1016/j.ymssp.2017.09.023**.

[13] Guo, Y., Parker, R. G., (2012). Stiffness matrix calculation of rolling element bearings using a finite element/contact mechanics model. *Mechanism and Machine Theory*, vol. 51, p. 32-45, **DOI:10.1016/j.mechmachtheory.2011.12.006**.

[14] Fang, B., Zhang, J., Yan, K., Hong, J., Yu Wang, M. (2019). A comprehensive study on the speed-varying stiffness of ball bearing under different load conditions. *Mechanism and Machine Theory*, vol. 136, p. 1-13, **DOI:10.1016/j.mechmachtheory.2019.02.012**.

[15] Razpotnik, M., Čepon, G., Boltežar, M. (2018). A smooth contact-state transition in a dynamic model of rolling-element bearings. *Journal of Sound and Vibration*, vol. 430, p. 196-213, **DOI:10.1016/j.jsv.2018.05.041**.

[16] Kabus, S., Hansen, M.R., Mouritsen, O. (2012). A new quasi-static cylindrical roller bearing model to accurately consider non-hertzian contact pressure in time-domain simulations. *Journal of Tribology*, vol. 134, no. 4, art. ID 041401, **DOI:10.1115/1.4007219**.

[17] Kabus, S., Hansen, M., Mouritsen, O. (2014). A new quasi-static multi-degree of freedom tapered roller bearing model to accurately consider non-Hertzian contact pressures in time-domain simulations. *Proceedings of the Institution of ol. Mechanical Engineers, Part K: Journal of Multi-body Dynamic*s, vol. 228, no. 2, **DOI:10.1177/1464419313513446**.

[18] Creju, S., Bercea, I., Mitu, N. (1995). A dynamic analysis of tapered roller bearing under fully flooded conditions. Part I: Theoretical formulation. *Wear*, vol. 188, no. 1-2, p. 1-10, **DOI:10.1016/0043-1648(94)06551-9**.

[19] Cretu, S., Mitu, N., Bercea, I. (1995). A dynamic analysis of tapered roller bearings under fully flooded conditions part 2: results. *Wear*, vol. 188, no. 1-2, p. 11-18, **DOI:10.1016/0043-1648(94)06552-7**.

[20] Tong, V.C., Hong, S.W. (2014). Characteristics of tapered roller bearing subjected to combined radial and moment loads. *International Journal of Precision Engineering and Manufacturing-Green Technology*, vol. 1, no. 4, p. 323-328, **DOI:10.1007/s40684-014-0040-1**.

[21] Tong, V.C., Hong, S.W. (2015). Effects of roller profile on the stiffness of tapered roller bearings. *Journal of Automation and Control Engineering*, vol. 3, no. 2, p. 151-156, **DOI:10.12720/joace.3.2.151-156**.

[22] Zhao, J.-S. Liu, W., Zhang, Y., Feng, Z.-J., Ye, J., Niu, Q.-B. (2013). Effects of gyroscopic moment on the damage of a tapered roller bearing. *Mechanism and Machine Theory*, vol. 69, p. 185-199, **DOI:10.1016/j.mechmachtheory.2013.06.002**.

[23] Roda-Casanova, V., Sanchez-Marin, F. (2017). Contribution of the deflection of tapered roller bearings to the misalignment of the pinion in a pinion-rack transmission. *Mechanism and Machine Theory*, vol. 109, p. 78-94, **DOI:10.1016/j.mechmachtheory.2016.11.013**.

[24] Houpert, L. (2002). Ball bearing and tapered roller bearing torque: analytical, numerical and experimental results. *Tribology Transaction*s, vol. 45, no. 3, p. 345-353, **DOI:10.1080/10402000208982559**.

[25] Ai, S., Wang, W., Wang, Y., Zhao, Z. (2015). Temperature rise of double-row tapered roller bearings analyzed with the thermal network method. *Tribology International*, vol. 87, p. 11-22, **DOI:10.1016/j.triboint.2015.02.011**.

[26] Tong, V.-C., Hong, S.-W. (2016). The effect of angular misalignment on the running torques of tapered roller bearings. *Tribology International*, vol. 95, p. 76-85, **DOI:10.1016/j.triboint.2015.11.005**.

[27] Zhou, R.S., Hoeprich, M.R. (1991). Torque of tapered roller bearings. *Journal of Tribology*, vol. 113, no. 3, p. 590-597, **DOI:10.1115/1.2920664**.

[28] Gradu, M. (2000). Tapered roller bearings with improved efficiency and high power density for automotive transmissions. *SAE 2020 World Congres*s, **DOI:10.4271/2000-01-1154**.

[29] Wrzochal, M., Adamczak, S., Domagalski, R., Piotrowicz, G., Wnuk, S. (2022). New device proposed for industrial measurement of rolling bearing friction torque. *Strojniški vestnik - Journal of Mechanical Engineering*, vol. 68, no. 10, p. 610-622, **DOI:10.5545/sv-jme.2022.275**.

[30] Zhang, J., Fang, B., Zhu, Y., Hong, J. (2017). A comparative study and stiffness analysis of angular contact ball bearings under different preload mechanisms, *Mechanism and Machine Theory*, vol. 115, p. 1-17, **DOI:10.1016/j.mechmachtheory.2017.03.012**.

[31] Altair Optistruct Eng. (2017). *Altair Optistruct Reference Guide*, Troy.

[32] Sheng, X., Li, B., Wu, Z., Li, H. (2014). Calculation of ball bearing speed-varying stiffness. Mechanism and Machine Theory, vol. 81, p. 166-180, **DOI:10.1016/j.mechmachtheory.2014.07.003**.